International Journal of Control, Automation and Systems 14(5) (2016) 1352-1364
http://dx.doi.org/10.1007/s12555-014-0452-2
ISSN:1598-6446 eISSN:2005-4092
http://www.springer.com/12555

Obstacle Avoidance with Translational and Efficient Rotational Motion Control Considering Movable Gaps and Footprint for Autonomous Mobile Robot

Ayanori Yorozu* and Masaki Takahashi

Abstract: This paper presents a sensor-based real-time obstacle avoidance method for an autonomous omnidirectional mobile robot based on simultaneous control of translational and efficient rotational motion considering movable gaps and the footprint. Autonomous mobile service robots that have been developed in recent years have arms that work and execute tasks. Depending on the task using moving parts, the shape of the robot (i.e., the footprint) changes. In this study, to improve the safety and possibility of reaching a goal even through a narrow gap with unknown obstacles, a sensor-based real-time obstacle avoidance method with simultaneous control of translational and efficient rotational motion (without unnecessary rotational motion) based on the evaluation of movable gaps and the footprint is proposed. To take account of the anisotropy footprint of the robot, multiple-circle robot model is proposed. In this paper, a novel control method based on fuzzy set theory is presented. To verify the effectiveness of the proposed method, several simulations and experiments are carried out.

Keywords: Autonomous mobile robot, fuzzy set theory, omnidirectional drive system, sensor-based real-time obstacle avoidance.

1. INTRODUCTION

Recently, autonomous mobile service robots that work in human living spaces have been studied and developed. It has been reported that several robots work in public facilities [1–3]. As shown in Fig. 1, these robots carry out tasks such as the transport of baggage or human assistance with moving parts such as arms [4–10]. Depending on the task using moving parts, the shape of the robot (i.e., the footprint) changes. To realize safe movement for unknown obstacles and humans, a sensor-based real-time obstacle avoidance method that considers the footprint is required.

Additionally, to realize smooth movement, the robots shown in Figs. 1(a) to (c) have an omnidirectional drive system that can control translational and rotational motion simultaneously. As shown in Fig. 2(a), if the robot is regarded as a circle in accordance with the conventional method [11–15], the robot cannot realize smooth movement to take advantage of the characteristics of the omnidirectional drive system because there is no change in the relation between the robot and surrounding environment with rotational motion. In an effort to solve this problem, the simultaneous control of translational and rotational motion considering the anisotropy footprint has been proposed and it has been reported that it is possible to improve the safety and possibility of reaching a goal [16–21]. A yaw angle of the robot is basically determined so as to enlarge the minimum distance between the robot model and obstacle [16–18]. In these methods, the robot is likely to rotate for obstacles even if the robot can move toward a goal while keeping a safe distance from obstacles. Most autonomous mobile robots move toward a goal with self-localization. However, it is well known that a movement with rotational motion has lower accuracy of self-localization than the movement without rotational motion. Thus, it is desirable for robots to head toward a goal without unnecessary rotational motion. Therefore, it is necessary to determine the suitable yaw angle in real time from the evaluation of the relation between movable gaps and the footprint.

In this study, to improve safety and the possibility of reaching a goal even through a narrow gap with unknown obstacles, we propose a sensor-based real-time obstacle

Manuscript received October 31, 2014; revised May 22, 2015 and August 24, 2015; accepted October 5, 2015. Recommended by Associate Editor Pinhas Ben-Tzvi under the direction of Editor Hyouk Ryeol Choi. This work was supported in part by Grant-in-Aid for Japan Society for the Promotion of Science Fellows Grant Number 25-5707 and Grant in Aid for the Global Center of Excellence Program for "Center for Education and Research of Symbiotic, Safe and Secure System Design" from the Ministry of Education, Culture, Sport, and Technology in Japan.

Ayanori Yorozu is with the School of Science for Open and Environmental Systems, Keio University, 3-14-1 Hiyoshi, Kohoku-ku, Yokohama 223-8522, Japan (e-mail: ayanoriyorozu@a5.keio.jp). Masaki Takahashi is with the Department of System Design Engineering, Keio University, 3-14-1 Hiyoshi, Kohoku-ku, Yokohama 223-8522, Japan (e-mail: takahashi@sd.keio.ac.jp).
* Corresponding author.

(a) MKR-003 for hospital use (b) TWENDY-ONE [7] (c) Rollin Justin [9] (d) Navy [10]

Fig. 1. Examples of autonomous mobile robots with arms that work in human living spaces.

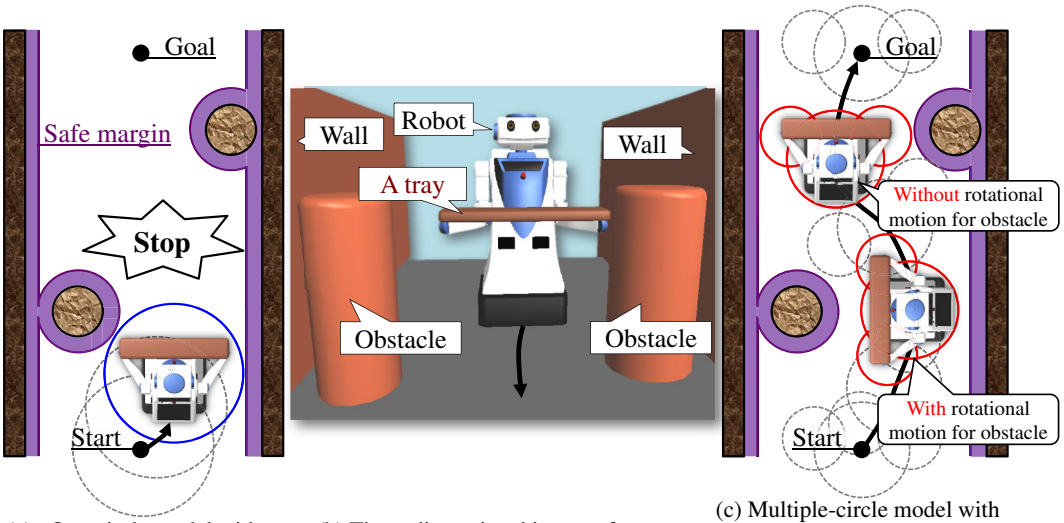

(a) One-circle model with translational motion (b) Three-dimensional image of a situation where a robot hold a tray (c) Multiple-circle model with translational and rotational motion based on the evaluation of the movable gaps and footprint

Fig. 2. Example of a situation that a robot needs to evaluate movable gaps and footprint.

avoidance method with simultaneous control of translational and efficient rotational motion based on the evaluation of movable gaps and the footprint. To take account of the anisotropy footprint of the robot that has moving parts, multiple-circle robot model is proposed. The main contribution of the proposed method is that the robot can keep a safe distance from obstacles even through a narrow gap and is able to reach a goal with efficient rotational motion (without unnecessary rotational motion) by determining a suitable yaw angle based on the evaluation of movable gaps and the proposed robot model. For example, with the proposed methods as shown in the avoidance for the first obstacle in Fig. 2(c), it is expected that the robot can keep a safe distance from obstacles and has the possibility of reaching the goal even through a narrow gap by changing the relation between the robot and the environment. Especially, as shown in the avoidance for the second obstacle in Fig. 2(c), determining the yaw angle from the evaluation of movable gaps and the footprint, it is also expected that the robot can head toward to the goal without unnecessary rotational motion if the robot can keep a safe distance from obstacles.

In this paper, we present an example of an obstacle avoidance method considering movable gaps and the footprint based on the sensor-based real-time simultaneous control of translational and efficient rotational motion using fuzzy set theory in reference [16]. To verify the effectiveness of the proposed robot model and simultaneous control of translational and rotational motion considering movable gaps and the robot model, several simulations and experiments are carried out.

2. ROBOT MODEL CONSIDERING MOVING PARTS

In this study, we propose a novel robot model with multiple circles for considering rotational motion with the omnidirectional drive system and the footprint of the robot depending on moving parts. In this study, we assumed that the robot does not hold the large baggage which sig-

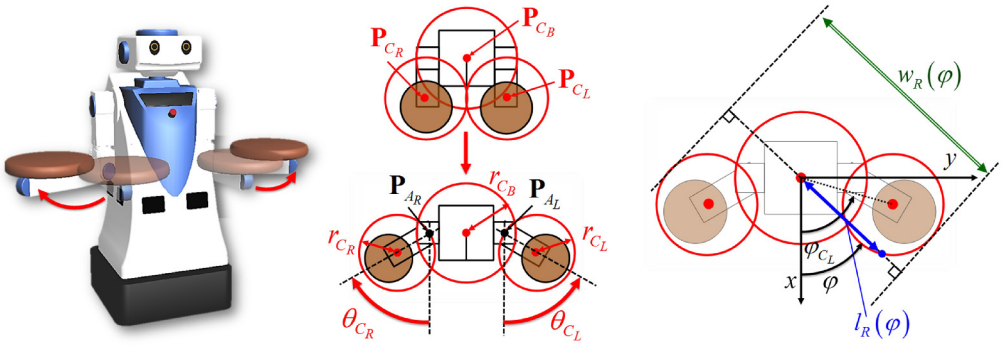

(a) Robot holds two trays (b) Parameters for motion control

Fig. 3. Example of the proposed robot model.

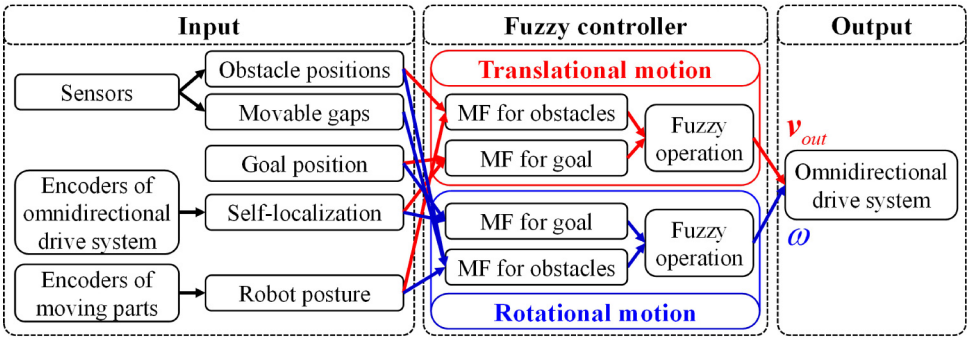

Fig. 4. Concept of simultaneous control of translational and rotational motion considering the evaluation of movable gaps and the robot model.

nificantly protrudes from the footprint of the moving parts considering the safety of transportation. Therefore, we introduce the modeling method which involves enclosing the robot body in a circle and enclosing moving parts in separate circles. Fig. 3 shows an example of the robot model with separate circles for each arm. $\mathbf{P}_{C_i}$ is the relative position from the center of the robot and r_{C_i} is the radius of the circle C_i. $\mathbf{P}_{A_i}$ is the relative position of the axis and θ_{C_i} is an angle of the moving part. $i = B, L, R$ indicates the body, left arm, and right arm respectively. The modeling method in a situation where the robot holds the large baggage is future work.

In addition, as shown in Fig. 3(b), to evaluate movable gaps and the robot model shown in Section 3, contour $l_R(\varphi)$ and width $w_R(\varphi)$ of the robot are defined as functions of φ, which is measured counterclockwise from the front of the robot and are calculated as

$$l_R(\varphi) = \max\left(\forall\sqrt{r_{C_i}^2 - \|\mathbf{P}_{C_i}\|^2 \sin^2(\varphi_{C_i} - \varphi)} + \|\mathbf{P}_{C_i}\|\cos(\varphi_{C_i} - \varphi)\right), \quad (1)$$

$$w_R(\varphi) = \max\left(\forall\|\mathbf{P}_{C_i}\|\cos(\varphi_{C_i} - \varphi) + r_{C_i}\right) - \min\left(\forall\|\mathbf{P}_{C_i}\|\cos(\varphi_{C_i} - \varphi) - r_{C_i}\right), \quad (2)$$

where φ_{C_i} is the relative direction of position $\mathbf{P}_{C_i}$ from the front of the robot.

3. SIMULTANEOUS CONTROL OF TRANSLATIONAL AND ROTATIONAL MOTION CONSIDERING MOVABLE GAPS AND THE ROBOT MODEL

With the proposed anisotropic robot model, it is possible to design a simultaneous control of translational and rotational motion with the omnidirectional drive system that can realize smooth movement while maintaining a safe distance from obstacles and allowing a goal to be reached even through narrow gaps. Additionally, because rotational motion is likely to decrease the accuracy of self-localization, it is desirable for the robot to head toward the goal without unnecessary rotational motion if the robot can keep a safe distance from obstacles. Therefore, it is necessary to determine the suitable yaw angle from the evaluation of movable gaps and the footprint. Since the robot can move the direction except the robot front, this study assumes that the robot is constantly scanning the whole environment to detect unknown obstacles and measure gaps.

In this study, we present an example of an obstacle avoidance method considering the movable gaps and the footprint based on the sensor-based real-time simultaneous control of translational and efficient rotational motion using fuzzy set theory in reference [16]. Fuzzy set theory

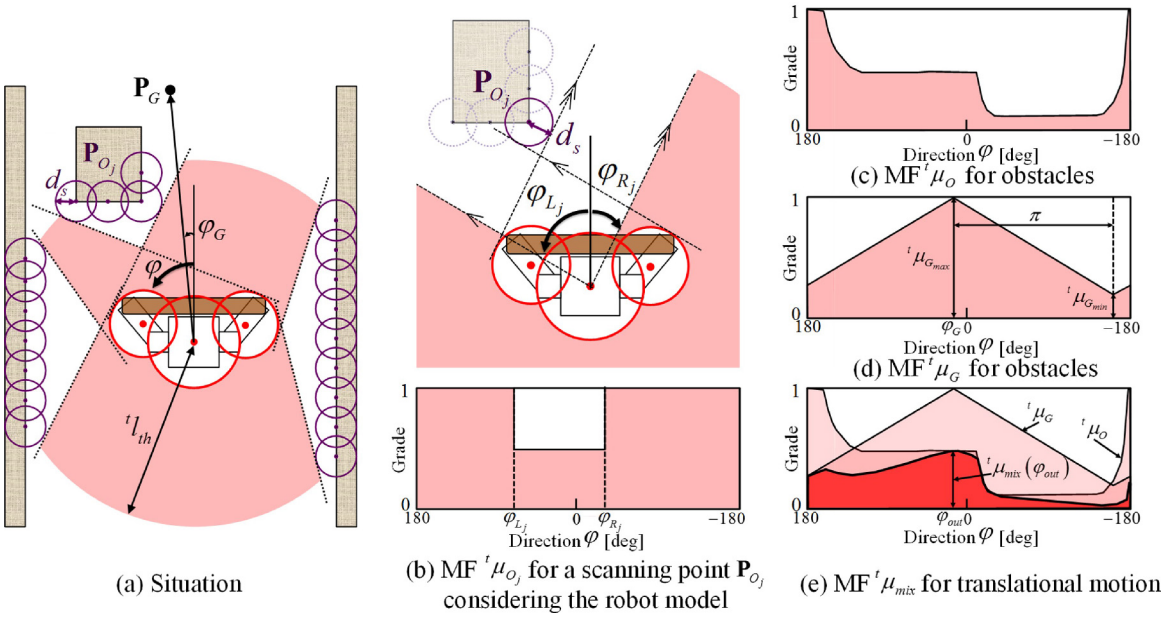

Fig. 5. Example of determination of translational motion.

has a characteristic that it is possible to take into account multiple-element action such as movement toward a goal and collision avoidance simultaneously using membership functions (MFs). Fig. 4 shows a concept of the simultaneous control of translational and rotational motion considering movable gaps and the proposed robot model.

The robot first obtains the posture of the robot and the environment data from the sensors. Membership functions for translational and rotational motion are then generated. The horizontal axis of an MF is the direction φ ranging from -180 to 180 degrees measured counterclockwise from the front of the robot. The vertical axis of an MF is the grade for the direction. The grade, direction, and configured maximum and minimum speeds are used to calculate the command velocity vector. Finally, translational and rotational velocity commands, which are calculated by defuzzification of mixed MFs, are realized by the omnidirectional drive system.

3.1. Translational motion considering the robot model and environment

For the robot model shown in Fig. 5 (a), translational MF is generated to move toward a goal while keeping a safe distance d_s from obstacles detected with sensors such as a laser range sensor (LRS).

3.1.1 Translational MF for obstacles

To enable a robot to avoid obstacles safely and efficiently in real time, the concave MF ${}^t\mu_{O_j}$ $(j = 1, ...,M)$ shown in Fig. 5(b), which takes into consideration the robot model, is generated. This MF is calculated from the geometrical relation between the robot model and the j-th sensor scanning point $\mathbf{P}_{O_j}$ with safe distance d_s:

$$ {}^t\mu_{O_j}(\varphi) = \begin{cases} \dfrac{\|\mathbf{P}_{O_j}\| - l_R(\varphi) - d_s}{{}^t l_{th} - l_R(\varphi) - d_s} & \text{if } \|\mathbf{P}_{O_j}\| < {}^t l_{th} \wedge \varphi_{L_j} \\ & < \varphi < \varphi_{R_j} \\ 1, & \text{otherwise,} \end{cases} \tag{3} $$

where φ_{L_j} and φ_{R_j} are the relative directions of the robot such that the robot does not collide with the scanning point $\mathbf{P}_{O_j}$ considering d_s as shown in Fig. 5(b). If the scanning point $\mathbf{P}_{O_j}$ is within a circle with radius ${}^t l_{th}$ from the robot, the MF ${}^t\mu_{O_j}$ is generated. For safe avoidance, the MF ${}^t\mu_O$ is generated for all scanning points that the robot detects. Then, as shown in Fig. 5(c), individual MFs are integrated into ${}^t\mu_O$ by calculating the logical product:

$$ {}^t\mu_O = {}^t\mu_{O_1} \wedge \cdots \wedge {}^t\mu_{O_M}. \tag{4} $$

3.1.2 Translational MF for a goal

To move toward a goal, a triangular MF ${}^t\mu_G$ is generated, as shown in Fig. 5(d). As a measure with which to decide how close to the goal the robot should go, ${}^t\mu_{G_{max}}$ is defined as the height of the triangular MF. As a measure with which to decide how much the robot can back away from obstacles, ${}^t\mu_{G_{min}}$ is defined. ${}^t\mu_G$ reaches a maximum value ${}^t\mu_{G_{max}}$ at the goal direction relative to the front of the robot φ_G:

$$ {}^t\mu_{G_{max}} = \begin{cases} \dfrac{\|P_G\|}{{}^t l_{th}} & \text{if } \|P_G\| \le {}^t l_{th} \\ 1 & otherwise, \end{cases} \tag{5} $$

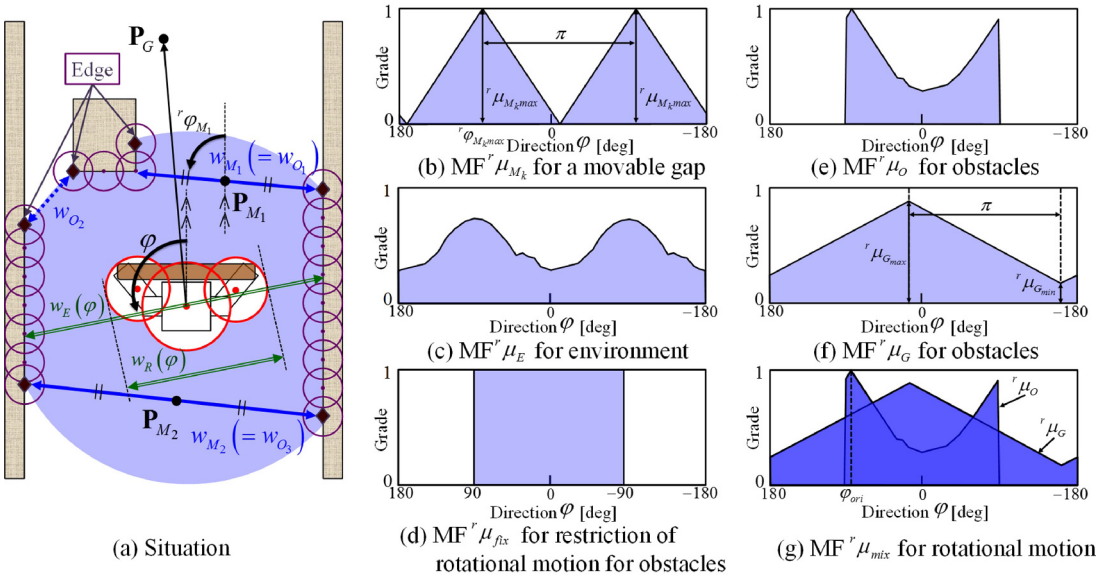

Fig. 6. Example of determination of rotational motion.

$$ {}^{t}\mu_{G_{min}} = {}^{t}\eta\,{}^{t}\mu_{G_{max}} \qquad (0 \le {}^{t}\eta < 1), \tag{6} $$

where $\|\mathbf{P}_G\|$ is the absolute value of the position vector of the goal relative to the robot. ${}^{t}\eta$ denotes constants. If $\|\mathbf{P}_G\|$ is less than ${}^{t}l_{th}$, ${}^{t}\mu_{G_{max}}$ is designed to be small. The robot can decelerate and stop stably at the goal.

3.1.3 Calculation of a translational command velocity vector

The proposed method uses fuzzy inference to calculate the translational command velocity vector. The MFs ${}^{t}\mu_{O}$ and ${}^{t}\mu_{G}$ are integrated by fuzzy operation into a mixed MF ${}^{t}\mu_{mix}$ as shown in Fig. 5(e). ${}^{t}\mu_{mix}$ is an algebraic product of ${}^{t}\mu_{O}$ and ${}^{t}\mu_{G}$:

$$ {}^{t}\mu_{mix} = {}^{t}\mu_{G} \cdot {}^{t}\mu_{O}. \tag{7} $$

Then, using a defuzzifier, a command velocity vector is calculated as a traveling direction φ_{out} and an absolute value of the reference speed v_{out} of the robot. From the mixed MF ${}^{t}\mu_{mix}$, φ_{out} and v_{out} are calculated:

$$ \varphi_{out} = \arg\max\left({}^{t}\mu_{mix}(\varphi)\right), \tag{8} $$

$$ v_{out} = {}^{t}\mu_{mix}(\varphi_{out}) \cdot v_{max}, \tag{9} $$

where v_{max} is the upper limit of the robot translational speed.

3.2. Rotational motion considering movable gaps and the robot model

To improve safety and the possibility of reaching a goal even through a narrow gap with unknown obstacles, rotational MF is generated to determine a suitable yaw angle in real time from the evaluation of the relation between movable gaps and the robot model.

3.2.1 Rotational MF for obstacles

If the robot is unable to move while keeping a safe distance d_s from obstacles and facing the goal, the rotational MF ${}^{r}\mu_{O}$ for obstacles, which takes into consideration of the width relation between movable gaps and the robot model and distance relation between the surrounding environment and the robot model, is generated. As shown in Fig. 6, ${}^{r}\mu_{O}$ is generated by the integration of MF ${}^{r}\mu_{M}$ for movable gaps and MF ${}^{r}\mu_{E}$ for the surrounding environment of the robot.

Firstly, to generate ${}^{r}\mu_{M}$, the robot detects the movable gaps from the distance data obtained with sensors such as an LRS according to reference [15]. Edges shown as diamonds in Fig. 6(a) are detected using the following equation with respect to the scanning point $\mathbf{P}_{O_j}$ ($j = 1, ..., M$) within the radius ${}^{r}l_{th}$ from the center of the robot; $\mathbf{P}_{O_j}$ is classified into several obstacles.

$$ \left\|\mathbf{P}_{O_j} - \mathbf{P}_{O_{j-1}}\right\| > 2d_s. \tag{10} $$

Minimum gaps between the scanning points of the neighboring obstacles are then defined as obstacles gaps w_{O_q} ($q = 1, ..., Q$) which are shown as dashed arrows in Fig. 6(a). If w_{O_q} satisfies

$$ w_{O_q} > \min\left(w_R(\varphi)\right) + 2d_s, \tag{11} $$

then w_{O_q} is identified as a movable gap w_{M_k} ($k = 1, ..., K$ ($K \le Q$)) which is shown as a solid arrow in Fig. 6(a).

As shown in Fig. 6(b), triangular MFs ${}^{r}\mu_{M_k}$ ($k = 1, ..., K$) for movable gaps w_{M_k} are generated considering the robot model. The maximum value ${}^{r}\mu_{M_k max}$ considering the

width $w_R(\varphi)$ of the robot model is calculated as

$$ {}^{r}\mu'_{M_k max} = \frac{\max(w_R(\varphi)) + 2d_s}{w_{M_k}} \cdot \frac{\|\mathbf{P}_G\|}{\|\mathbf{P}_{M_k}\| + \|\mathbf{P}_G - \mathbf{P}_{M_k}\|}, \tag{12} $$

$$ {}^{r}\mu_{M_k max} = \frac{1}{\max\left(1,\ \forall {}^{r}\mu'_{M_k max}\right)} \cdot {}^{r}\mu'_{M_k max}, \tag{13} $$

where $\mathbf{P}_{M_k}$ is the relative center position of w_{M_k} from the center of the robot. ${}^{r}\varphi_{M_k max}$ is the relative direction from the direction for which the width $w_R(\varphi)$ of the robot model is a minimum and is obtained as

$$ {}^{r}\varphi_{M_k max} = {}^{r}\varphi_{M_k} - \arg\min(w_R(\varphi)), \tag{14} $$

where ${}^{r}\varphi_{M_k}$ is the relative direction from the front of the robot as shown in Fig. 6(a).

Secondly, as shown in Fig. 6(c), rotational MF ${}^{r}\mu_E$ for the surrounding environment considering the safe distance is generated as

$$ {}^{r}\mu_E(\varphi) = \frac{w_R(\varphi - \arg\min(w_R(\varphi))) + 2d_s}{w_E(\varphi - \arg\min(w_R(\varphi)))}, \tag{15} $$

where $w_E(\varphi)$ is the width of the environment based on the sensor data shown as a doublet arrow in Fig. 6(a).

Finally, as shown in Fig. 6(e), for rotational motion to keep a safe distance from obstacles, the rotational MF for obstacles is a logical sum of ${}^{r}\mu_{M_k}$ ($k = 1, ..., K$) and ${}^{r}\mu_E$:

$$ {}^{r}\mu_O = ({}^{r}\mu_{M_1} \vee \cdots \vee {}^{r}\mu_{M_K} \vee {}^{r}\mu_E) \wedge {}^{r}\mu_{fix}, \tag{16} $$

where ${}^{r}\mu_{fix}$ is a MF not to select the direction more than 90 degree for obstacles as shown in Fig. 6(d).

3.2.2 Rotational MF for a goal

To turn the front of the robot toward the goal direction φ_G if there is no obstacle to avoid, rotational MF ${}^{r}\mu_G$ for a goal is generated as shown in Fig. 6 (f). Triangular MF ${}^{r}\mu_G$ reaches a maximum value ${}^{r}\mu_{G_{max}}$ at the goal direction relative to the front of the robot φ_G. ${}^{r}\mu_{G_{max}}$ is designed to be greater if the robot model is able to ensure a safe distance from obstacles and the surrounding environment. The minimum value ${}^{r}\mu_{G_{min}}$ is designed to have a constant value ${}^{r}\eta$ ($0 \leq {}^{r}\eta < 1$) such as ${}^{t}\mu_{G_{min}}$.

$$ {}^{r}\mu_{G_{max}} = \min\left(1, \forall \frac{1}{{}^{r}\mu'_{M_k max}}, \forall \frac{\min(w_E(\varphi))}{\max(w_R(\varphi)) + 2d_s}\right), \tag{17} $$

$$ {}^{r}\mu_{G_{min}} = {}^{r}\eta\, {}^{r}\mu_{G_{max}} \quad (0 \leq {}^{r}\eta < 1). \tag{18} $$

3.2.3 Calculation of a rotational command velocity vector

For rotational motion, like translational motion, the rotational command velocity vector is derived. As shown in Fig. 6 (g), the MFs ${}^{r}\mu_O$ and ${}^{r}\mu_G$ are integrated by a fuzzy operation into a mixed MF ${}^{r}\mu_{mix}$ for rotational motion. ${}^{r}\mu_{mix}$ is a logical sum of ${}^{r}\mu_O$ and ${}^{r}\mu_G$:

$$ {}^{r}\mu_{mix} = {}^{r}\mu_G \vee {}^{r}\mu_O. \tag{19} $$

Then, using a defuzzifier, a rotational command velocity vector is calculated as a rotational direction φ_{ori} and an absolute value of the reference rotational speed ω of the robot. From the mixed MF ${}^{r}\mu_{mix}$, φ_{ori} and ω are calculated:

$$ \varphi_{ori} = \arg\max({}^{r}\mu_{mix}(\varphi)), \tag{20} $$

$$ \omega = \frac{\varphi_{ori}}{\pi} \cdot \omega_{max}, \tag{21} $$

where ω_{max} is the upper limit of the robot rotational speed.

Finally, the translational and rotational velocity commands are realized simultaneously by an omnidirectional drive system [16].

4. SIMULATIONS

To verify the effectiveness of the proposed robot model and obstacle avoidance method, several numerical simulations were carried out. In the simulation, the robot was assumed to transport baggage with arms as shown in Fig. 1. As shown in Fig. 7, the robot has an omnidirectional drive system and can measure omnidirectional range up to 4.0 m every 100 ms with two LRSs (URG-04LX, Hokuyo Automatic Co, Ltd. [22]). The parameters $d_s = 0.2$, ${}^{t}l_{th} = {}^{r}l_{th} = 2.0$, and ${}^{t}\eta = {}^{r}\eta = 0.2$ were set.

4.1. Verification of the robot model and changing yaw angle

This section verifies the relation between the robot and the environment due to the moving parts and the change in yaw angle. As shown in Fig. 8, there were two static obstacles with radii of 0.40 m in the field and the robot was assumed to transport a tray from an initial position (0.0 m, 0.0 m) to a goal position (3.0 m, 0.0 m). In situations A1 to A7, the robot was assumed to hold a tray with

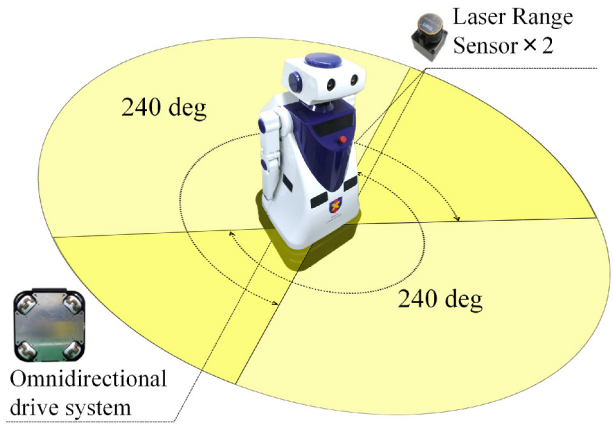

Fig. 7. System of the robot.

Table 1. Parameters of the robot model of situations A1 to B2 in simulations of Section 4.1.

Robot model	r_{C_B} [m]	r_{C_L} [m]	P_{A_L} [m]	r_{C_R} [m]	P_{A_R} [m]
Conventional (One circle)	0.60	–	–	–	–
Proposal (Multiple circle)	0.35	0.25	(0.0, 0.25)	0.25	(0.0, -0.25)

Table 2. Parameters of situations A1 to B2 in simulations of Section 4.1.

Situation	Robot model				Environment
	θ_{C_L} [deg]	θ_{C_R} [deg]	ψ [deg]	w_R [m]	w_G [m]
A1	–	–	0.0	1.20	1.50
A2	0.0	0.0	0.0	1.00	1.50
A3	0.0	0.0	0.0	1.00	1.30
A4	0.0	0.0	90.0	0.85	1.30
A5	0.0	0.0	90.0	0.85	1.20
A6	45.0	45.0	0.0	1.35	1.20
A7	45.0	45.0	90.0	0.78	1.20
B1	90.0	0.0	90.0	0.85	1.20
B2	90.0	0.0	72.0	0.76	1.20

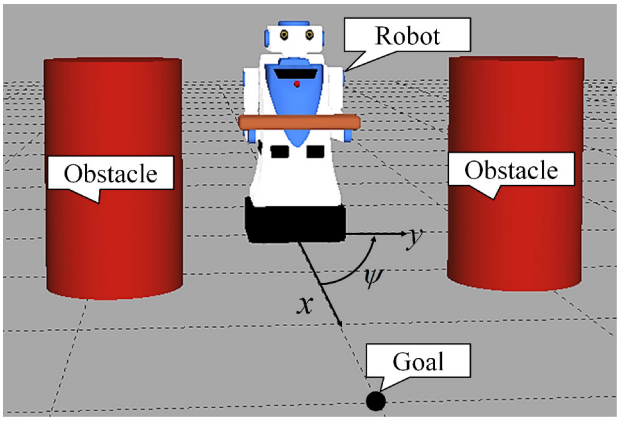

Fig. 8. Three-dimensional image of the field.

arms and the footprint of the robot was symmetrical as shown in Figs. 1(b) and 1(c). In situations B1 and B2, the robot was assumed to hold a tray with its left arm and the footprint of the robot was asymmetrical as shown in Fig. 1(d). We verified the change in the traveling direction due to the position of the arms and yaw angle with MF ${}^t\mu_{mix}$ for translational motion in these situations. Table 1 gives the parameters of the robot model. The yaw angle ψ of the robot, width w_R of the robot with respect to the goal direction, and gap w_G of the two obstacles are shown in Table 2.

In situation A1 shown in Fig. 9(a), the robot determined the traveling direction to detour the obstacles because the relation between the gap and the width of the robot was $w_G(=1.50) < w_R + 2d_s(=1.20+2\times0.20=1.60)$. In addition, if the robot was regarded as one circle, the robot could not realize smooth movement using the omnidirectional drive system because there is no change in the relation between the robot and environment with rotational motion. On the other hand, in situation A2 shown in Fig. 9(b), the robot could pass between the obstacles because the relation was $w_G(=1.50) > w_R + 2d_s(=1.00+2\times0.20=1.40)$. In situation A3 shown in Fig. 9(c), the robot determined the traveling direction to detour the obstacles because the relation was $w_G(=1.30) < w_R + 2d_s(=1.00+2\times0.20=1.40)$. On the other hand, in situation A4 shown in Fig. 9(d), the robot could pass between the obstacles because the relation changed to $w_G(=1.30) > w_R + 2d_s(=0.85+2\times0.20=1.25)$ with a change in the yaw angle.

In situations A6 and A7, the robot was assumed to hold a tray that was longer than that in situations A1 to A5. Figs. 9(f) and 9(g) confirms that the robot could change its traveling direction by also changing the yaw angle in situations A2 and A3. Additionally, in situation A5 shown in Fig. 9(e), the robot determined the traveling direction to detour the obstacles even if it changed the yaw angle because the relation was $w_G(=1.20) < w_R + 2d_s(=0.85+2\times0.20=1.25)$. On the other hand, in situation A7 where the arms of the robot were different from those in situation A5, the robot could pass between the obstacles because the relation was $w_G(=1.20) > w_R + 2d_s(=0.78+2\times0.20=1.18)$.

Moreover, in situation B1 shown in Fig. 9(h) where the robot model was asymmetrical and $\psi = 90.0$, the robot determined the traveling direction to detour the obstacles because the relation was $w_G(=1.20) < w_R + 2d_s(=0.85+2\times0.20=1.25)$ as well as situation A5. On the other hand, in situation B2 shown in Fig. 9(i), the robot could pass between the obstacles because the relation changed to $w_G(=1.20) > w_R + 2d_s(=0.76+2\times0.20=1.16)$ with a

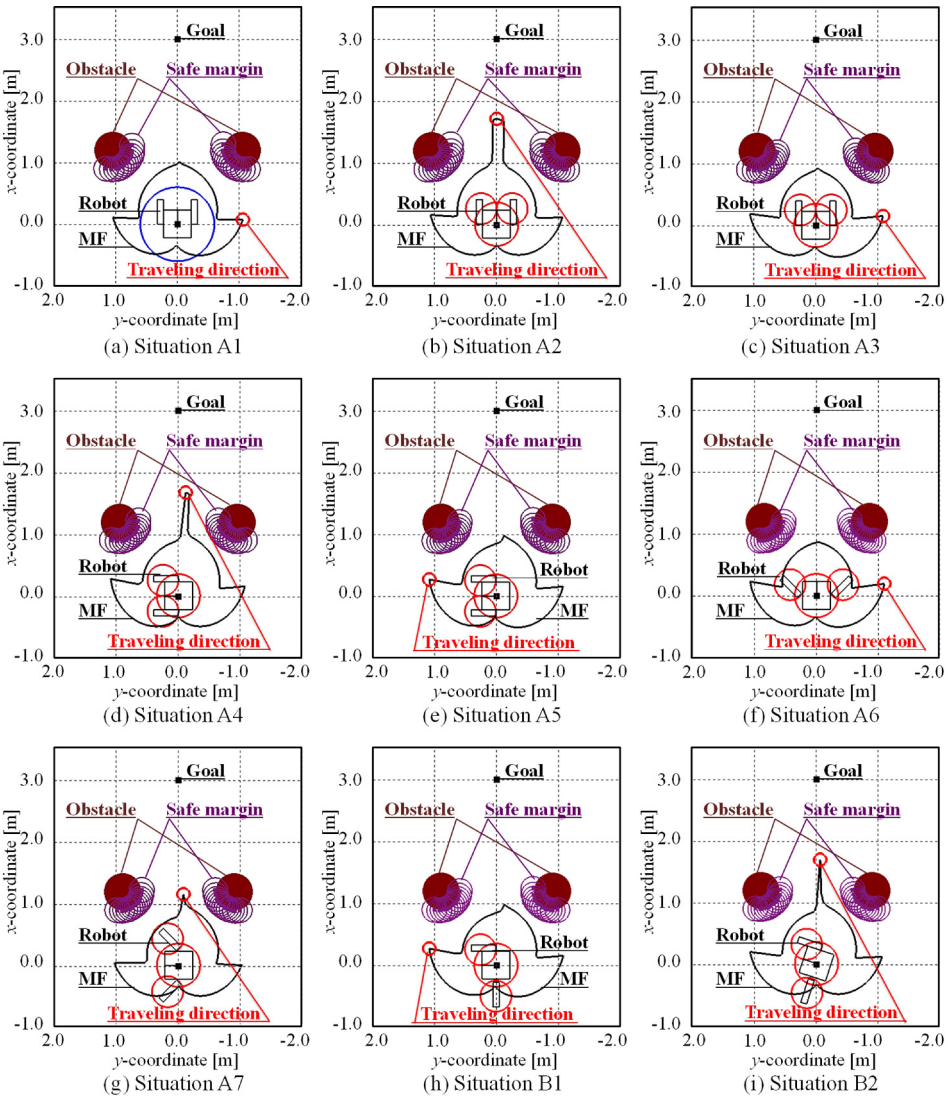

Fig. 9. Simulation results of the translational MF and the traveling direction depending on the robot model and rotational motion in Section 4.1.

change in the yaw angle in consideration of the minimum width of the asymmetrical robot model.

These results confirm that the proposed multiple-circle robot model is able to take into account the various footprints of the robot depending on the task and thereby an obstacle avoidance method considering the advantage of the omnidirectional drive system can be designed.

4.2. Verification of rotational motion based on the evaluation of movable gaps and the robot model

This section verifies the safety in obstacle avoidance and the effectiveness of the rotational motion based on the evaluation of the movable gaps and the footprint. As shown in Fig. 10, there were three static obstacles in a passage of 2.4 m width. The robot was assumed to transport a tray from the initial position (0.0 m, 0.0 m) to the goal position (7.0 m, 0.0 m). It was assumed that the robot was able to realize self-localization, but had no priori information about the obstacles. Then, the maximum translational speed v_{max} was 0.5 m/s and the translational acceleration was 0.5 m/s^2, and the maximum rotational speed ω_{max} was 60 deg/s and the rotational acceleration was 60 deg/s^2. Other parameters are given in Table 3. Fig. 10 shows the trajectory of the robot every 2.0 s, Fig. 11 shows the time history of the yaw angle, and Table 4 gives the closest approach distance from the robot to the walls and obstacles.

As shown in Fig. 10(a), the robot could pass the obstacle 1 because the relation between the width of the robot model and the gap w_{G_2} between the obstacle 1 and the left was $w_{G_1}(=1.90) > \min(w_R(\varphi)) + 2d_s(=1.40+2\times0.20=1.80)$. However, the robot did not reach the goal because the relation between the width of the robot model and the gap w_{G_2} between the obstacle 2 and the right wall

Table 3. Parameters of conventional and proposed methods in simulations of Sections 4.2 and experiments.

	Rotational motion	Robot model				
		r_{C_B} [m]	r_{C_L}, r_{C_R} [m]	θ_{C_L}, θ_{C_R} [deg]	$\max(w_R(\varphi))$ [m]	$\min(w_R(\varphi))$ [m]
Conventional method	No	0.70	–	–	1.40	1.40
Proposed method	Yes	0.35	0.25	45.0	1.35	0.78

Table 4. Closest approach distance from the robot to the walls and obstacles with the proposed method in simulation of Section 4.2.

	Left wall	Right wall	Obstacle 1	Obstacle 2	Obstacle 3
Distance [m]	0.32	0.26	0.20	0.21	0.20

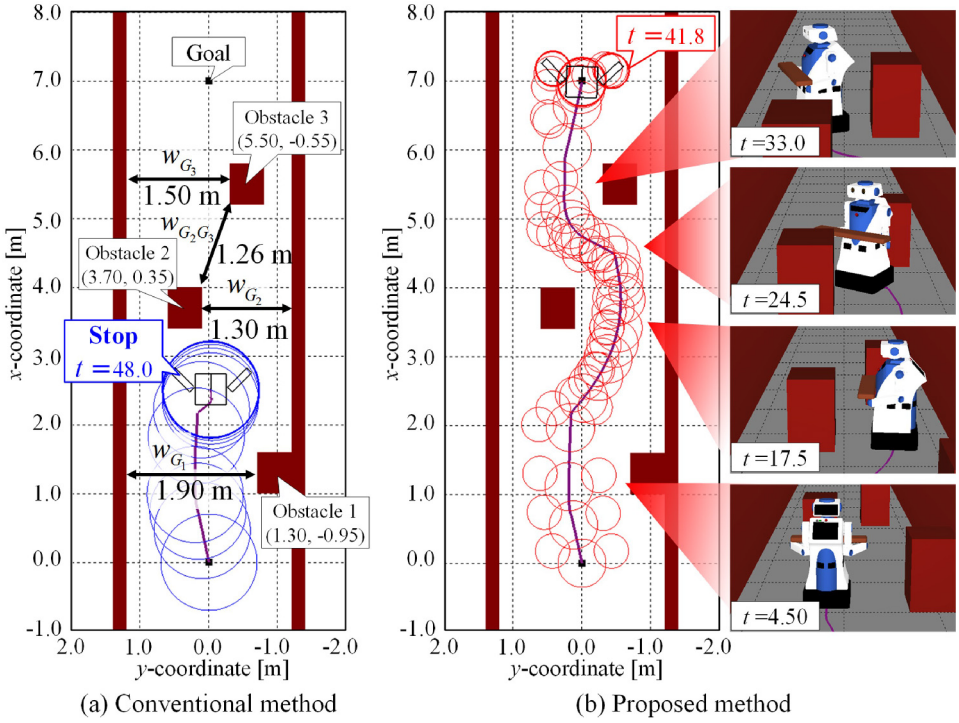

(a) Conventional method (b) Proposed method

Fig. 10. Simulation results of the robot trajectory in Section 4.2.

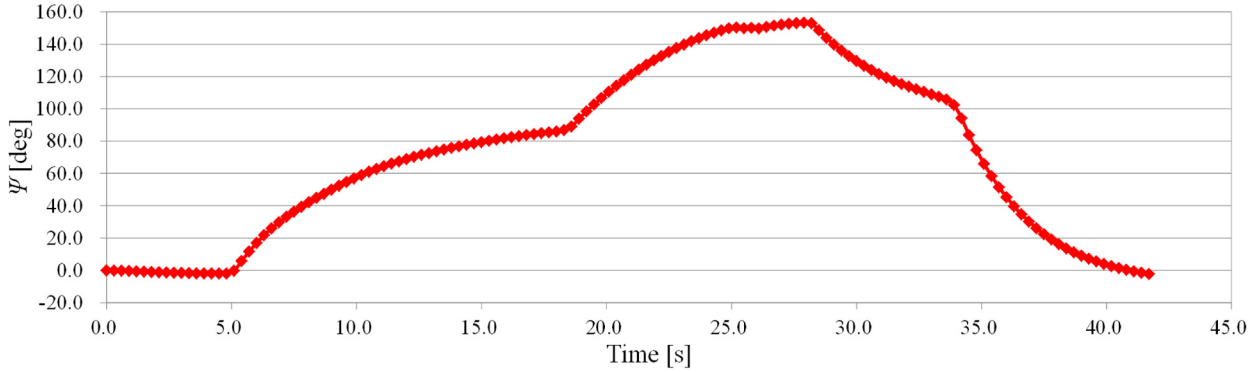

Fig. 11. Time history of the robot yaw angle with the proposed method in simulation of Section 4.2.

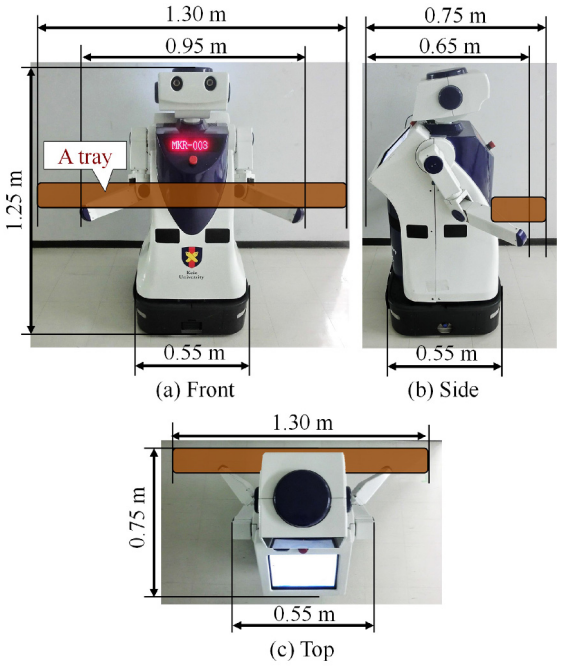

Fig. 12. Experimental situation of the robot.

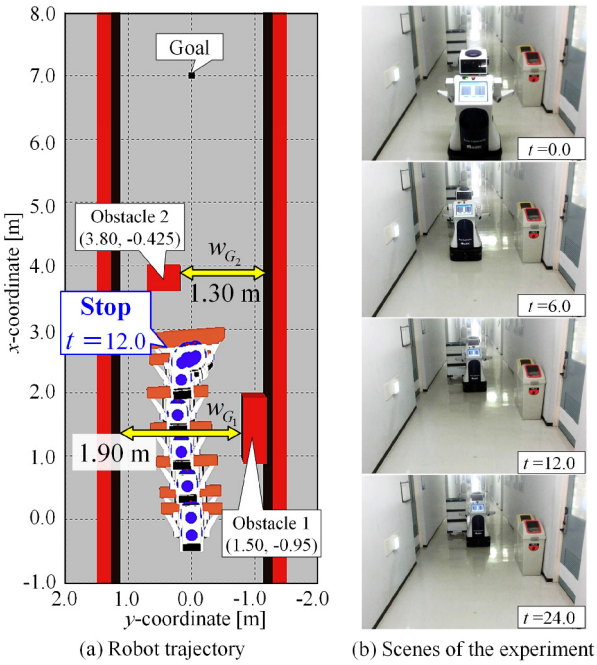

Fig. 13. Experimental results with the conventional method.

was $w_{G_2}(=1.30) < \min(w_R(\varphi)) + 2d_s(=1.40+2\times0.20=1.80)$ with a circle model.

As shown in Fig. 10(b), the robot could pass obstacle 1 without rotational motion because the gap w_{G_1} between the obstacle 1 and the left wall was $w_{G_1}(=1.90) > \min(w_R(\varphi)) + 2d_s(=1.35+2\times0.20=1.75)$. In addition, the robot could pass obstacle 2 with rotational motion because the relation between the minimum width $w_R(\varphi)$ of the robot andw_{G_2} was $w_{G_2}(=1.30) > \min(w_R(\varphi)) + 2d_s(=1.18+2\times0.20=1.18)$. Moreover, the gap $w_{G_2G_3}$ between obstacles 2 and 3 and the gap w_{G_3} between the obstacle 3 and the left wall were too narrow for the robot to maintain a safe distance without rotational motion. As shown in Figs. 10(b) and 11 and Table 4, the robot could reach the goal while keeping a safe distance from all obstacles and walls by determining a suitable yaw angle according to the evaluation of movable gaps. These results confirmed that the robot could realize smooth movement to keep a safe distance from obstacles and the proposed simultaneous control of translational and rotational motion based on the evaluation ofmovable gaps and the proposed robot model improved the possibility of reaching a goal. It was also confirmed that the robot could move toward the goal without unnecessary rotational motion if the robot could keep a safe distance from obstacles.

5. EXPERIMENTS

To verify the effectiveness of the proposed robot model and obstacle avoidance method in practice, experiments using a real robot were carried out. In this study, we used an omnidirectional mobile robot called MKR-003 as shown in Fig. 7. The robot can measure omnidirectional range up to 4.0 m every 0.1 s with two LRSs (URG-04LX, Hokuyo Automatic Co, Ltd. [22]). The command velocity vector of the robot is realized by four DC motors and omni-wheels [23].

The robot was assumed to transport a tray as shown in Fig. 12. As shown in Fig. 13, there were two static obstacles in a passage of 2.25 m width. The robot moved to the goal position (7.0 m, 0.0 m) from the initial position (0.0 m, 0.0 m). The robot had a map of the passage and sequentially processed localization and calculated the command velocity, but had no priori information about the obstacles. The maximum translational speed v_{max} and the maximum rotational speed ω_{max} were set to 0.5 m/s and 60 deg/s respectively. Each parameter was shown in Table 3. Other parameters $d_s = 0.2$, ${}^t l_{th} = {}^r l_{th} = 2.0$, and ${}^t\eta = {}^r\eta = 0.2$ were set. Figs. 13 and 14 show the trajectory and scenes of the robot with the conventional and proposed method respectively. Fig. 15 shows the time history of the yaw angle with the proposed method.

As shown in Fig. 13, the robot could pass the obstacle 1 because the relation between the width of the robot model and the gap w_{G_2} between the obstacle 1 and the left was $w_{G_1}(=1.90) > \min(w_R(\varphi)) + 2d_s(=1.40+2\times0.20=1.80)$. However, the robot did not reach the goal because the relation between the width of the robot model and the gap w_{G_2} between the obstacle 2 and the right wall was $w_{G_2}(=1.30) < \min(w_R(\varphi)) + 2d_s(=1.40+2\times0.20=1.80)$ with a circle model.

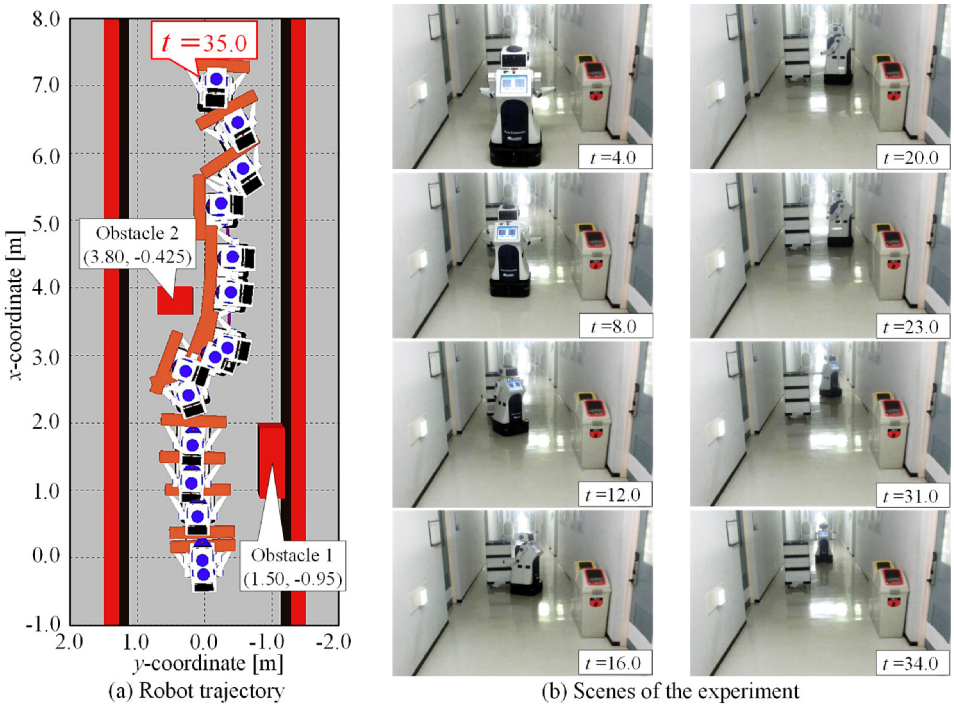

(a) Robot trajectory (b) Scenes of the experiment

Fig. 14. Experimental results of the robot trajectory.

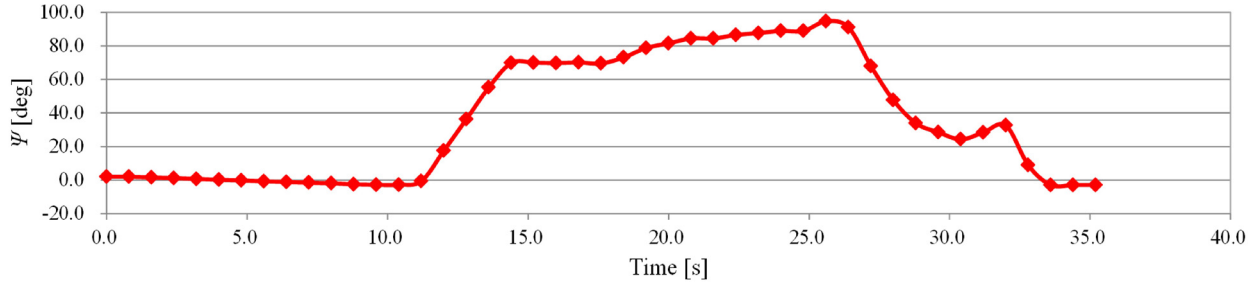

Fig. 15. Time history of the robot yaw angle with the proposed method in experiment.

As shown in Figs. 14 and 15, the robot could pass obstacle 1 without rotational motion because the gap w_{G_1} between the obstacle 1 and the left wall was w_{G_1} $(= 1.90) >$ $\max(w_R(\varphi)) + 2d_s$ $(= 1.75)$. In addition, the robot could pass obstacle 2 with rotational motion because the relation between the minimum width $w_R(\varphi)$ of the robot and w_{G_2} was w_{G_2} $(= 1.30) >$ $\min(w_R(\varphi)) + 2d_s$ $(= 1.18)$. These experimental results confirmed the effectiveness of the proposed method in practice.

6. CONCLUSION

This study proposed a sensor-based real-time obstacle avoidance method for an autonomous omnidirectional mobile robot with moving parts based on simultaneous-control of translational and efficient rotational motion considering movable gaps and the footprint. To take account of the anisotropy footprint of the robot that has moving parts, multiple-circle robot model was also proposed. The main contribution of this study is that the robot can keep a safe distance from obstacles even through a narrow gap and reach a goal with efficient rotational motion (without unnecessary rotational motion) by determining a suitable yaw angle based on the evaluation of movable gaps and the proposed robot model. To verify the effectiveness of the proposed method, several simulations and experiments in environments with unknown obstacles were carried out. From these results, it was confirmed that the proposed method could realize smooth movement to keep a safe distance from obstacles and could improve the possibility of reaching a goal without unnecessary rotational motion.

Moreover, in addition to translational and rotational motion, if the robot can change the positions of its moving parts while it is moving, it is expected that the robot will be more flexible in various situations. Therefore, an

obstacle avoidance method considering this point is future work.

REFERENCES

[1] J. M. Evans, "HelpMate: An autonomous mobile robot courier for hospitals," *Proc. of IEEE/RSJ/GI International Conference on Intelligent Robots and Systems*, pp. 1695-1700, 1994.

[2] M. Bennewitz, W. Burgard, A. B. Cremers, F. Dellaert, D. Fox, D. Hahnel, C. Rosenberg, N. Roy, J. Schulte, and D. Schulz, "MINERVA: A second-generation museum tour-guide robot," *Proc. of IEEE International Conference on Robotics and Automation*, pp. 1999-2005, 1999.

[3] B. Jensen, N. Tomatis, L. Mayor, A. Drygajlo, and R. Siegwart, "Robots meet humans – Interaction in public spaces," *IEEE Transactions on Industrial Electronics*, vol. 52, no. 6, pp. 1530-1546, 2005. [click]

[4] Z. Tiejun, T. Dalong, and Z. Mingyang, "The development of a mobile humanoid robot with varying joint stiffness waist," *Proc. of IEEE International Conference Mechatronics and Automation*, pp.1402-1407, 2005.

[5] S. R. Kuindersm, E. Hannigan, D. Ruiken, and R. A. Grupen, "Dexterous mobility with the uBot-5 mobile manipulator," *Proc. of IEEE International Conference on Advanced Robotics*, pp. 1-7, 2009.

[6] J. S. Mehling, P. Strawser, L. Bridgwater, W. K. Verdeyen, and R. Rovekamp, "Centaur: NASA's mobile humanoid designed for field work," *Proc. of IEEE International Conference on Robotics and Automation*, pp. 2928-2933, 2007. [click]

[7] H. Iwata and S. Sugano, "Design of human symbiotic robot TWENDY-ONE," *Proc. of IEEE International Conference on Robotics and Automation*, pp. 580-586, 2009. [click]

[8] T. Asfour, K. Regenstein, P. Azad, J. Schroder, A. Bierbaum, N. Vahrenkapm, and R. Dillmann, "ARMAR-III: An integrated humanoid platform for sensory-motor control," *Proc. of IEEE-RAS International Conference on Humanoid Robots*, pp. 169-175, 2006. [click]

[9] M. Fuchs, C. Borst, P. R. Giordano, A. Baumann, E. Kraemer, J. Langwald, R. Gruber, N. Seitz, G. Plank, K. Kunze, R. Burger, F. Schmidt, T. Wimboeck, and G. Hizinger, "Rollin' Justin – Design considerations and realization of a mobile platform for a humanoid upper body," *Proc. of IEEE International Conference on Robotics and Automation*, pp. 4131-4137, 2009.

[10] Tmsuk Co., Ltd., http://www.tmsuk.co.jp/lineup/aidu/index.html, (accessed of October 20, 2014).

[11] J. Borenstein and Y. Koren, "The vector field histogram fast obstacle avoidance for mobile robots," *IEEE Transactions on Robotics and Automation*, vol. 7, no. 3, pp. 278-288, 1991. [click]

[12] D. Fox, W. Burgard, and S. Thrun, "The dynamic window approach to collision avoidance," *IEEE Robotics and Automation Magazine*, vol. 4, no. 1, pp. 23-33, 1997. [click]

[13] J. Minguez, L. Montano, "Nearness diagram (ND) navigation: Collision avoidance in troublesome scenarios," *IEEE Transactions on Robotics and Automation*, vol. 20, no. 1, pp. 45-59, 2004.

[14] J. Minguez, "The obstacle-restriction method (ORM) for robot obstacle avoidance in difficult environments," *Proc. of IEEE International Conference on Robotics and Automation*, pp. 2284-2290, 2005.

[15] M. Mujahad, D. Fischer, B. Mertsching, H. Jaddu, "Closest gap based (CG) reactive obstacle avoidance navigation for highly cluttered environments," *Proc. of IEEE/RSJ International Conference on Intelligent Robots and Systems*, pp. 1805-1812, 2010. [click]

[16] T. Suzuki and M. Takahashi, "Translational and rotational motion control considering width for autonomous mobile robots using fuzzy inference," *Numerical Analysis Theory and Application, InTech Book*, pp. 563-576, 2011.

[17] S. Ito, M. Shimizu, H. Yamato, K. Irie, T. Furuta, and Y. Hayasbibara, "Obstacle avoidance algorithm with potential method considering robot shape," *JEME Conference on Robotics and Mechatronics* (in Japanese), 2010.

[18] A. Nagata, K. Nonaka, and K. Sekiguchi, "Model predictive obstacle avoidance control for omni-directional mobile robots based on fuzzy potential method," *Proc. of European Control Conference*, pp. 352-357, 2014. [click]

[19] A. Yorozu, T. Suzuki, T. Matsumura, and M. Takahashi, "Simultaneous control of translational and rotational motion for autonomous omnidirectional mobile robot considering shape of the robot and movable area by heights," *Intelligent Autonomous Systems 12*, *Advances in intelligent Systems and Computing*, vol. 193, pp. 91-100, 2013. [click]

[20] C. Sprunk, B. Lau, P. Pfaff, and W. Burgard, "Online generation of kinodynamic trajectories for non-circular omnidirectional robots," *Proc. of IEEE International Conference on Robotics and Automation*, pp. 72-77, 2011. [click]

[21] M. Dakulović, C. Sprunk, L. Spinello, I. Petrović, and W. Burgard, "Efficient navigation for anyshape holonomic mobile robots in dynamic environments," *Proc. of IEEE/RSJ International Conference on Intelligent Robots and Systems*, pp. 2644-2649, 2013.

[22] Hokuyo Automatic Co, Ltd., http://www.hokuyo-aut.jp/, (accessed of October 20, 2014).

[23] M. Takahashi, T. Suzuki, H. Shitamoto, T. Moriguchi, and K. Yoshida, "Developing a mobile robot for transport applications in the hospital domain," *Robotics and Autonomous Systems*, vol. 58, no. 7, pp. 889-899, 2010. [click]

Ayanori Yorozu received his B.E. degree from the Department of System Design Engineering and M.E. degree in the School of Science for Open and Environmental Systems from Keio University, in 2011 and 2013. His research interests include mobile robot navigation and human tracking. He is a member of Japan Society of Mechanical Engineers and The Robotics Society of Japan.

Masaki Takahashi received hid B.E. and M.E. degrees from the Department of System Design Engineering at Keio University, in 2000 and 2002, respectively. He received the D.Eng. degree from Keio University, Yokohama, Japan, in 2004. In 2004, he started working as a Research Assistant of the 21st Century COE Program: "System Design: Paradigm shift from Intelligence to Life". From 2005 to 2008, he worked as a Research Assistant of the Department of System Design Engineering, Keio University, Yokohama, Japan and became an Associate Professor in 2009. His primary research interests include human-robot interaction, motion and vibration control, and sensor fusion. He is a member of American Institute of Aeronautics and Astronautics, The Japan Society of Mechanical Engineers and The Robotics Society of Japan.